frontiers | Frontiers in Nuclear Engineering

TYPE Original Research
PUBLISHED 22 January 2024
DOI 10.3389/fnuen.2023.1340426

Check for updates

OPEN ACCESS

EDITED BY
Tonya Vitova,
Karlsruhe Institute of Technology (KIT), Germany

REVIEWED BY
Charles M. Folden,
Texas A&M University, United States
Ningappa C.,
Vidya Vikas Institute of Engineering and Technology, India

*CORRESPONDENCE
Tashiema L. Ulrich,
ulrichtl@ornl.gov

†Present address:
Tashiema L. Ulrich,
Nuclear Energy and Fuel Cycle Division, Nuclear Fuel Development Section, Nuclear Fuel Performance Group, Oak Ridge National Laboratory, Oak Ridge, TN, United States

RECEIVED 17 November 2023
ACCEPTED 28 December 2023
PUBLISHED 22 January 2024

CITATION
Ulrich TL and Besmann TM (2024), Phase equilibria of advanced technology uranium silicide-based nuclear fuel.
Front. Nucl. Eng. 2:1340426.
doi: 10.3389/fnuen.2023.1340426

Phase equilibria of advanced technology uranium silicide-based nuclear fuel

Tashiema L. Ulrich*† and Theodore M. Besmann

Department of Mechanical Engineering, Nuclear Engineering Program, University of South Carolina, Columbia, SC, United States

The phases in uranium-silicide binary system were evaluated in regards to their stabilities, phase boundaries, crystal structures, and phase transitions. The results from this study were used in combination with a well assessed literature to optimize the U-Si phase diagram using the CALPHAD method. A thermodynamic database was developed, which could be used to guide nuclear fuel fabrication, could be incorporated into other nuclear fuel thermodynamic databases, or could be used to generate data required by fuel performance codes to model fuel behavior in normal or off-normal reactor operations. The U_3Si_2 and U_3Si_5 phases were modeled using the Compound Energy Formalism model with 3 sublattices to account for the variation in composition. The crystal structure used for the USi phase was the tetragonal with an *I4/mmm* space. Above 450°C, the U_3Si_5 phase was modeled. The composition of the USi_2 phase was adjusted to $USi_{1.84}$. The calculated invariant reactions and the enthalpy of formation for the stoichiometric phases were in agreement with experimental data.

KEYWORDS

uranium silicides, phase diagram, CALPHAD, nuclear fuel, U3Si2, U3Si5

1 Introduction

The tsunami-initiated nuclear accident that occurred at Fukushima, Japan a decade ago was the impetus behind the world's renewed interest in alternative fuel concepts with enhanced accident tolerance for the current fleet of commercial power reactors (U.S. Nuclear Regulatory Commission, 2011; Kim et al., 2016; Zinkle and Was, 2013; Karoutas et al., 2018; Kurata, 2016). In the United States, the Department of Energy's Office of Nuclear Energy initiated the accident tolerant fuel (ATF) development program, within the Advanced Fuels Campaign (AFC), to identify alternative fuel technologies to further enhance the safety and competitiveness of commercial nuclear power (U.S Department of Energy, 2015; Carmack et al., 2013; Bragg-Sitton et al., 2014; Terrani, 2018).

The U-Si system contains several compounds that are of interest as either a monolithic replacement for the current UO_2 fuel (White et al., 2015; Goddard et al., 2016; World Nuclear News, 2019; Johnson et al., 2020; Westinghouse, 2023), a composite fuel with UN (Johnson et al., 2016; White et al., 2017; Wilson et al., 2018) or metal fuel (Dwight, 1982; Kim and Konings, 2012). The U-Si system has been the subject of various studies detailing thermophysical properties (White et al., 2014; White et al., 2015; White et al., 2015; White et al., 2016). The phase equilibria and thermodynamic properties of the U-Si system has been assessed by Berche et al. (2009) and Wang et al. (2016) however there are concerns regarding the accuracy and completeness of the phase diagram (Remschnig et al., 1992; Berche et al., 2009; White et al., 2015; Middleburgh et al., 2016; Noordhoek et al., 2016; Wang et al., 2016; Lopes et al., 2018; Wilson et al., 2018; Kocevski et al., 2019; Ulrich et al.,

2020a; Ulrich et al., 2020b). Companion compositions to U_3Si_2 and U_3Si_5 require further study for a fuller understanding of compositional changes expected to occur in silicide fuel during reactor operation. These include compositions in the range of the USi and $USi_{1.88}$ phases which lie within the 40–66 at% Si region of the phase diagram and can be considered as potential high burn-up phases. Questions remain concerning phase transition, homogeneity range, crystal structure, and potentially new equilibrium phases. As such, further experimental efforts have been suggested (Berche et al., 2009; White et al., 2015; Wilson et al., 2018).

The aim of this project was to develop a self-consistent thermodynamic database for the uranium-silicon system by 1) performing targeted experimental analyses of the potential U_3Si_5 phase transition, homogeneity range for the U_3Si_2, U_3Si_5 and the $USi_{1.88}$ phases, the crystal structure of USi and the stability of the U_5Si_4 and U_2Si_3 phases; 2) using density functional theory (DFT) and molecular dynamics (MD) simulations to predict the energetically and dynamically stable phases in the U-Si system; 3) coupling the computational and experimental results with data from a critically assessed literature to optimize the U-Si system using the CALculation of PHAse Diagram (CALPHAD) method; 4) building and validating a U-Si thermodynamic model. The database generated from this work could be used with other fuel performance codes to predict silicide fuel behavior during normal or off-normal reactor operations, optimize fuel fabrication processes, and support licensing efforts. The focus of this paper is the optimized U-Si phase diagram from the theoretical and experimental data generated from this project as well as literature data.

2 Literature review

2.1 U-Si phase diagram

The first compositional diagram for the uranium-silicon system was based on studies performed by Kaufmann et al., in the 1940s at the Massachusetts Institute of Technology (Cullity, 1945). The original phases reported were $U_{10}Si_3$, U_5Si_3, USi, U_2Si_3, USi_2, and USi_3 (Katz and Rabinowitch, 1951). In 1949, Zachariasen (1949) further refined the original composition diagram by correcting the identification of several compounds; $U_{10}Si_3$ was actually U_3Si, U_5Si_3 was U_3Si_2, and U_2Si_3 (β-USi_2) was an isostructural form of USi_2 (α-USi_2).

Later, in 1957, Kaufmann et al. (1957) published the phase diagram shown in Figure 1A, which contains the compounds U_3Si (ε), U_3Si_2 (δ), USi (ζ), U_2Si_3 (η), USi_2 (θ) and USi_3 (ι). Kaufmann et al. (1957) claimed that the ε phase has a very narrow composition range near 23 at% Si, rather than a stoichiometric ratio of U_3Si and also that the α-USi_2 phase did not transform at high temperature to β-USi_2 and formed the compound U_2Si_3 in its place. U_3Si forms at 1203 K through the peritectic reaction between U_3Si_2 and γ-uranium-silicon solid solution. A eutectic exists between γ-uranium and U_3Si_2 at 9 at% Si and a temperature of 1258 K. The compound U_3Si_2 congruently melts at 1938 K. The USi compound incongruently melts at 1848 K and there is a eutectic between U_3Si_2 and USi at 1843 K. The U_2Si_3 compound incongruently melts at 1883 K and the USi_2 compound is reported to melt congruently at approximately 1973 K. USi_3 is shown to have an incongruent melting point at 1783 K. There is a eutectic at 87 at% Si between USi_3 and silicon at 1588 K. There was appreciable solid solubility of silicon in uranium.

The phase diagram that is currently referenced is shown in Figure 1B and was published in 1990 in ASM international (Massalski, 1990). This phase diagram is characterized by seven intermetallic phases, U_3Si, U_3Si_2, USi, U_3Si_5, $USi_{1.88}$, USi_2, and USi_3. The 0–50 at% Si region remained as previously reported by Kaufmann et al. (1957) except for the temperature where the eutectic reaction occurs between U_3Si_2 and USi. The phase identified as U_2Si_3 by Kaufmann, or β-USi_2 by Zachariasen (1949), is represented as U_3Si_5. In 1959 Brown and Norreys (1959) reported that the U_2Si_3 phase was in fact a modification of the α-USi_2 compound; however, the composition was located between 62–63 at% Si (U_3Si_5). Brown and Norreys (1961) also reported that the phase considered as α-USi_2 is actually $USi_{1.88}$, forming at 65 at% Si and has high melting point. They further claimed that the compound at exact 1:2 stoichiometry does not exist above 723 K.

In an attempt to elucidate the controversy regarding the phases between the 40 to70 at% silicon region of the U-Si system, Vaugoyeau et al. (1972) reexamined the system within this region. The existence of compounds USi, U_3Si_5, U_3Si_2 and $USi_{1.88}$ were confirmed (Vaugoyeau et al., 1972). Vaugoyeau et al. (1972) reported: The USi phase forms at 1853 ± 10 K from a peritectic reaction between liquid and U_3Si_5. The temperature of the eutectic reaction between USi and U_3Si_2 was 1813 ± 10 K, which is approximately 20 K lower than that reported by Kaufmann et al., (Kaufmann et al., 1957). The melting of U_3Si_5 occurred congruently at 2043 ± 10 K instead of incongruently at 1883 K. The $USi_{1.88}$, reported by Brown and Norreys (1961) forms through a peritectic reaction between liquid and U_3Si_5 at 1983 ± 10 K. The stoichiometric USi_2 compound was not observed by Vaugoyeau et al. (1972).

Additional research since the publication of the phase diagram in Figure 1B shows the need for updates. The U_3Si phase was reported to undergo an allotropic transition at 1043 K (Dwight, 1982). A new phase, U_5Si_4, was reported by Noël et al. (1998) and Berche et al. (2009) claimed that the phase is formed through a peritectic reaction between the liquid phase and U_3Si_2 at 1840 ± 10 K and participates in the eutectic reaction between the liquid phase and the USi phase at 1820 ± 10 K. The stoichiometric USi_2 phase was reported as metastable (Sasa and Uda, 1976; Dwight, 1982; Remschnig et al., 1992; Noordhoek et al., 2016) and the U_3Si_5, U_3Si_2, and $USi_{1.88}$ phases were each reported to have a narrow composition range (Dwight, 1982). A phase transition at 773 K was noted for the U_3Si_5 phase (White et al., 2015).

2.2 Crystallography

The crystal structure properties including the structure types, space groups, prototypes, lattice parameters for the various uranium silicide phases are summarized Table 1. The U_3Si crystal structure reported by Zachariasen (1949) in 1949 was often reproduced (Kaufmann et al., 1957; Dwight, 1982; Remschnig et al., 1992).

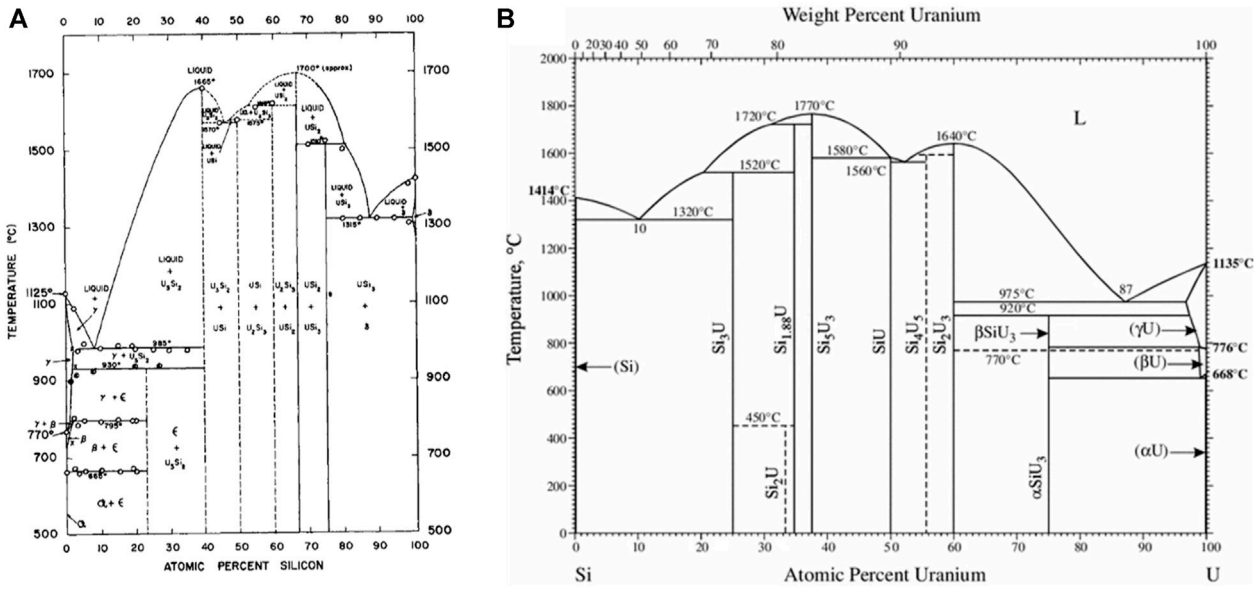

FIGURE 1
Illustration of the 1957 U-Si phase diagram **(A)** compared to the U-Si phase diagram currently referenced **(B)** (Kaufmann et al., 1957; Massalski, 1990).

Kimmel et al. (Kimmel et al., 1980), established that the space group reported earlier (Zachariasen, 1949) was correct; but the assignment of the uranium and silicon lattice sites was incorrect. Noël et al. (2023) also reported that the tetragonal structure undergoes an orthorhombic distortion at 120 K. Dwight, (1982) reported that the tetragonal U_3Si transforms to a cubic Cu_3Au-type structure at 1038 K.

The U_3Si_2 compound has a primitive tetragonal structure belonging to the *P4/mbm* space group and is a prototype for binary ternary rare earth compounds (Pöttgen, 1994; Lukachuk and Pöttgen, 2003). While all published experimental data are in agreement with the early work of Zachariasen (1949), DFT calculations fail to predict the experimental *P4/mbm* as the most stable structure (Noordhoek et al., 2016).

The U_5Si_4 phase reported in 1998 by Noël et al. (1998) has a hexagonal unit cell, *P6/mmm* space group, with lattice parameters a = 10.468 Å and c = 3.912 Å and is isostructural to the $U_{20}Si_{16}C_3$ ternary phase (Lopes et al., 2019; Noël et al., 2023). The crystal structure of the equiatomic compound, USi, is the most controversial of the binary silicides. The compound was reported by Zachariasen (1949) to be orthorhombic of the FeB structure type. His results were based on diffractometer data taken on a powder sample. In later work, Bihan et al. (1996) reported that pure USi has a tetragonal structure with an *I4/mmm* space group as determined from a Weissenberg pattern on a small single crystal. Bihan et al. (1996) further state that the orthorhombic structure by found by Zachariasen (1949) is stabilized by 0.5–1.0 wt% oxygen. Remschnig et al. (1992) and Noordhoek et al. (2016) also reported an orthorhombic structure; however, both differ from the work of Zachariasen, (1949) and each other as the structure by Remschnig et al. (1992) belongs to the *Pnma* space group while the one by Noordhoek et al. (2016) belongs to the *Imma* Space group.

The compound USi_2 with exact 1:2 stoichiometry has all silicon sites occupied and exists in one of two structure types, either AlB_2 or $ThSi_2$, belonging to the *P6/mmm* or the *I4₁/amd* space group. The compound U_3Si_5 is hexagonal, hP3, $A1B_2$-type structure which was reported to undergo an orthorhombic distortion when slightly rich in silicon (63 at% Si) to form the structure belonging to the *Pmmm* space group (Remschnig et al., 1992). The $USi_{1.88}$ phase is tetragonal of the $ThSi_2$-type and experiences an orthorhombic distortion when slightly silicon poor (64 at% Si) (Remschnig et al., 1992).

The silicon-rich compound USi_3 has the cubic Cu_3Au-type structure.

2.3 Thermodynamic values

The tabulated enthalpies of formation for the different U-Si phases are summarized in Table 2. The enthalpies of formation of USi_3, USi_2, USi and U_3Si_2 were measured as −33.05 kJ mol^{-1}, -43.51 kJ mol^{-1}, -40.17 kJ mol^{-1} and -33.89 kJ mol^{-1} by Gross et al. (1962) by measuring the heats evolved in the direct combination of the elements. The enthalpies of formation for USi_3, USi_2, and USi were verified by measuring the heats of reaction of tellurium with the preformed compounds and comparing them with those obtained from reacting equivalent quantities of the uncombined elements with tellurium. The enthalpy of formation for USi_3, USi_2, and USi were measured as −32.22, −42.69, and −43.52 kJ mol^{-1}, respectively (Gross et al., 1962). Alcock and Grieveson (1961) measured silicon vapor pressure above the mixtures USi-U_3Si_5, U_3Si_5–USi_2, USi_2–USi_3 and USi_3–Si from the weight loss of a Knudsen cell. From these measurements, the Gibbs energy of U_3Si_5, USi_2 and USi_3 were directly derived. Activities of uranium and silicon for the U–U_3Si_2 mixture were determined from the chemical analysis of the condensate formed from the vapor effusing from the cell.

TABLE 1 Summary of crystallographic properties for the U-Si phases including structure type, space group, prototype, and lattice parameters found in the literature.

Phase	Structure type	Space group	Prototype	Lattice parameters (Å)			Ref.
				a	b	c	
U_3Si (γ)	Cubic	*Pm-3m*	Cu_3Au	4.346	-	-	Massalski (1990)
U_3Si (β)	Tetragonal	*I4/mcm*	U_3Si (β)	6.0328	-	8.6907	Massalski (1990)
U_3Si (δ)	Tetragonal	*I4/mcm*	-	6.029 (2)	-	8.697 (3)	Zachariasen (1949)
U_3Si	Tetragonal	*I4/mcm*	U_3Si	6.029 (2)	-	8.696 (3)	Zachariasen (1949)
				6.033 (1)	-	8.688 (1)	Boucher (1971)
				6.0328	-	8.6907	Vooght et al. (1973)
U_3Si	Orthorhombic	*Fmmm*	U_3Si	8.654 (2)	8.523 (2)	8.523 (2)	Kimmel et al. (1980)
U_3Si (α)	Orthorhombic	*Fmmm*	U_3Si (α)	8.654	8.549	8.523	Massalski (1990)
U_3Si_2	Tetragonal	*P4/mbm*	U_3Si_2	7.3298 (4)	-	3.9003 (5)	Massalski (1990)
				7.3364 (5)	-	3.8900 (8)	Remschnig et al. (1992)
				7.3299	-	3.9004	Zachariasen (1949)
				7.3297	-	3.9003	Laugier et al. (1971)
U_5Si_4	Hexagonal	*P6/mmm*	$U_{20}Si_{16}C_3$	10.467	-	7.835	Noël et al. (1998)
USi	Tetragonal	*I4/mmm*	USi	10.58	-	24.310	Remschnig et al. (1992)
USi	Orthorhombic	*Pnma*		7.585	3.903	5.663	Remschnig et al. (1992)
USi	Orthorhombic	*Imma*		7.585	3.903	5.663	Noordhoek et al. (2016)
USi	Orthorhombic	*Pbmn*	FeB	5.66 (1)	7.67 (1)	3.91 (1)	Zachariasen (1949)
USi	Tetragonal	*I4/mmm*	USi	10.61	24.42	27.490	Laugier et al. (1971)
U_3Si_5	Hexagonal	*P6/mmm*	AlB_2	3.843	-	4.069	Massalski (1990)
				3.8475 (7)		4.074 (1)	Remschnig et al. (1992)
				3.843 (1)		4.069 (1)	Brown and Norreys (1959)
				3.890	6.660	4.040	Dwight, 1982a
o1-U_3Si_5 (at 63 at. % Si)	Orthorhombic	*Pmmm*	Dist. AlB_2	3.869		4.073	Remschnig et al. (1992)
o2-U_3Si_5 (at ~63 at% Si)	Orthorhombic	*Pmmm*	Dist. AlB_2	3.893	6.717	4.042	Remschnig et al. (1992)
USi_{2-z} (at 64 at. % Si)	Orthorhombic	*Imma*	Def. $GdSi_2$	3.953	3.929	13.656	Remschnig et al. (1992)
USi_{2-z} (at 65 at. % Si)	Tetragonal	*$I4_1/amd$*	Def. $ThSi_2$	3.9423	-	13.712	Zachariasen (1949), Remschnig et al. (1992)
$USi_{1.88}$	Tetragonal	*$I4_1/amd$*	Def. $ThSi_2$	3.9457 (4)	-	13.739 (7)	Remschnig et al. (1992)
				3.9378 (7)	-	13.729 (6)	Remschnig et al. (1992)
				3.948	-	13.67	Wilson et al. (2018)
				3.98 (3)	-	13.74 (8)	Zachariasen (1949)
USi_3	Cubic	*Pm-3m*	Cu_3Au	4.060	-	-	Zachariasen (1949)
USi_3	Cubic	*Pm3m*	L12 Cu_3Au	4.03	-	-	Kaufmann et al. (1957)
USi_3	Cubic	*Pm-3m*	Cu_3Au	4.0348 (8)	-	-	Ott et al. (1985)
USi_2	Tetragonal	*$I4_1/amd$*	$ThSi_2$	3.922	-	14.154	Zachariasen (1949)
USi_2	Tetragonal	*$I4_1/amd$*	$ThSi_2$	3.98 (3)	-	13.74 (8)	Zachariasen (1949)
USi_2	Hexagonal	*P6/mmm*	AlB_2	3.86 (1)	-	4.07 (1)	Zachariasen (1949)

(Continued on following page)

TABLE 1 (*Continued*) Summary of crystallographic properties for the U-Si phases including structure type, space group, prototype, and lattice parameters found in the literature.

Phase	Structure type	Space group	Prototype	Lattice parameters (Å)			Ref.
				a	b	c	
USi_2	Tetragonal	*I4₁/amd*	$ThSi_2$	3.97	-	13.71	Kaufmann et al. (1957)
USi_2	Cubic	-	-	4.053	-	-	Brauer and Haag (1949)
USi_2	Tetragonal	*I4₁/amd*	$ThSi_2$	3.9406 (7)	-	13.778 (7)	Remschnig et al. (1992)
USi_2	Tetragonal	*I4₁/amd*	$ThSi_2$	3.922	-	14.154	Sasa and Uda (1976)
				3.930	-	14.06	Brown and Norreys (1959)
					-		
USi_2	Hexagonal	*P6/mmm*	AlB_2	4.028 (1)	-	3.852 (1)	Brown and Norreys (1961)
$U_{22}Si_{78}$	Cubic	*Pm3m*	Cu_3Au	4.0353 (4)	-	-	Remschnig et al. (1992)

Because of small associated values of uranium activity, a solid/liquid equilibration method using liquid gold–uranium alloys were used for the U_3Si_2–USi mixture. The Gibbs energies of formation of the compounds were derived from the silicon and uranium activity measurements. The results reported by Gross et al. (1962) and Alcock and Grieveson (1961) are in good agreement. OHare et al. (1974) reported the enthalpy of formation of U_3Si as −26.05 ± 4.8 kJ mol-atom^{-1} using fluorine bomb calorimetry. The enthalpy of formation for U_3Si_5 and the tetragonal USi were measured as −43.8 ± 9.0 kJ mol $^{-1}$ and −43.2 ± 6.2 kJ mol $^{-1}$ for using oxidative drop calorimetry (Chung et al., 2018). The heat capacity as a function of temperature for U_3Si, U_3Si_2, USi and U_3Si_5 were measured by White et al. (2015); White et al. (2016) using differential scanning calorimetry from room temperature to 1150 K, 1773 K, 1673 K, and 1773 K, respectively. To the authors knowledge, there are no experimental efforts reported for obtaining the thermodynamic properties of the liquid phase.

3 CALPHAD methodology

3.1 General description of CALPHAD method

The CALPHAD method is commonly used for calculating phase diagrams and predicting thermodynamic properties of a given system through critical assessment of available experimental and/or theoretical data. The CALPHAD method uses mathematical models with adjustable parameters to represent Gibbs energy functions of the phases as a function of temperature, pressure, and composition and calculates the thermodynamic equilibrium by minimizing the Gibbs energy of the system (Kaufman and Bernstein, 1970; Lukas et al., 2007). These functions are stored in a database and are used to calculate phase diagrams and thermodynamic properties. These databases are constructed by incorporating phase diagram data, thermochemical data, and physical and crystallographic properties of the phases (Perrut, 2015).

The first step in the CALPHAD method is to perform a thorough literature search and critically evaluate all the available data. The type of data to search for include; i) experimentally measured thermodynamic quantities such as enthalpies and heat capacity data, ii) the phase diagram data such as the liquidus temperatures and the phase transition reactions, iii) crystallographic information of solid phases (Ferro and Cacciamani, 2002), and first-principles calculations of total energies (Liu, 2009). When evaluating the experimental data, critical attention is paid to the experimental technique, experimental conditions, sample purity, quantities measured, phases present within the system, and accuracy of the measurements as there are many types of equipment utilized to collect the same information. First-principles data are normally used when there are no available experimental data. During the literature search, the possibility of finding previous assessments for the system of interest exists. In such cases, careful examination of the Gibbs energy models used for describing the system is necessary as it may be possible to improve the system. The second step is to develop a mathematical model for G (T, P, composition) for each phase (liquid, solid phases, gas . . .) and to optimize model parameters simultaneously using all available thermodynamic and phase equilibrium data obtained from the first step. The third step is to use the models to calculate phase diagrams and other thermodynamic properties by minimization of the Gibbs energy. The fourth and final step is to use the calculated phase equilibria to develop a database.

3.2 Thermodynamic models

The Gibbs energy of a phase can be expressed as follows in Eqs 1, 2:

$$G_m = {}^{ref}G_m + {}^{id}G_m + {}^{E}G_m + {}^{phy}G_m \quad (1)$$

$${}^{id}G_m = -T\,{}^{id}S \quad (2)$$

Where ${}^{ref}G_m$ is the "surface of reference", which represents the Gibbs energy of the mechanical mixture of the constituents of the phase. ${}^{id}G_m$ is the contribution of configuration entropy to the Gibbs energy. T is the absolute temperature in Kelvin and ${}^{id}S$ is the configuration entropy, which is determined by the number of

TABLE 2 Summary of the enthalpy of formation for the various U-Si phases from the literature compared to the values calculated in this work.

Phase	ΔH_f (kJ/mol-atom) 298K	Method	References
USi_3	−33.02 ± 0.13	Direct comb. cal	Gross et al. (1962)
	−32.19 ± 0.84	Tellurium cal	Gross et al. (1962)
	−35.53 ± 4.18	Activity meas	Alcock and Grieveson (1961)
	−32.60	Estimation	Birtcher et al. (1989)
	−32.90	Modelling	Berche et al. (2009)
	−32.90	CALPHAD	This work
USi_2	−43.47 ± 0.42	Direct comb. Cal	Gross et al. (1962)
	−42.64 ± 1.25	Tellurium cal	Gross et al. (1962)
	−43.89 ± 4.18	Activity meas	Alcock and Grieveson (1961)
	−43.19	Estimation	Birtcher et al. (1989)
	−43.33	Modelling	Berche et al. (2009)
	−45.12	CALPHAD	This work
U_3Si_5	−44.26	Estimation	Birtcher et al. (1989)
	−42.9	Modelling	Berche et al. (2009)
	−43.8 ± 9.0	Oxidative drop cal	Chung et al. (2018)
USi	−40.13 ± 0.84	Direct comb. cal	Gross et al. (1962)
	−43.47 ± 1.67	Tellurium Cal	Gross et al. (1962)
	−41.8 ± 4.18	Activity meas	Alcock and Grieveson (1961)
	−42.22	Estimation	Birtcher et al. (1989)
	−41.18	Modelling	Berche et al. (2009)
	−43.2 ± 6.2	Oxidative drop cal	Chung et al. (2018)
	−41.78	CALPHAD	This work
U_3Si_2	−33.2 ± 3.1	High Temp Drop cal	Chung et al. (2018)
	−33.86 ± 0.42	Direct comb. cal	Gross et al. (1962)
	−35.95 ± 3.34	Activity meas	Birtcher et al. (1989)
	−34.11	Estimation	Alcock and Grieveson (1961)
	−34.32	Modelling	Berche et al. (2009)
U_3Si	−26.02 ± 4.8	Fluorine bomb cal	OHare et al. (1974)
	−22.99	Estimation	Birtcher et al. (1989)
	−24.93	Modelling	Berche et al. (2009)
	−24.91	CALPHAD	This work

possible arrangements of the constituents in a phase. ${}^{E}G_m$ is the excess Gibbs energy, the Gibbs energy change from the ideal solution to the real solution. ${}^{phy}G_m$ represents the Gibbs energy contribution of physical phenomena, such as magnetic transitions.

3.2.1 The gas phases

The gases in the U-Si system are Si_g, U_g, $Si_{(2g)}$ and $Si_{(3g)}$ gases. The Gibbs energy functions for the gases are taken from the Scientific Group Thermodata Europe (SGTE) database complied by Dinsdale for pure elements (Dinsdale, 1991).

3.2.2 Elements

The molar Gibbs energy ${}^{\circ}G_i$ of a pure element i in a phase at temperature and pressure of 10^5 Pa, relative to the "Standard Element Reference" H_i^{SER}, is described by a power series such as shown in Eq. 3:

$$ {}^{\circ}G_i - H_i^{SER} = a_0 + a_1 T + a_2 T ln(T) + a_3 T^2 + a_4 T^3 + a_5 T^{-1} + \ldots, T_1 < T < T_2 \quad (3) $$

$a_0, a_1, a_2, a_3, \ldots$ are coefficients, H_i^{SER} is the enthalpy of the pure element i in its reference state. Since the Gibbs energy has no absolute value, it is

TABLE 3 Phases, composition, crystal structure, and thermodynamic model used for the optimization of the U-Si phase diagram.

Phase	At% Si	Pearson symbol	Space group	Struktur-bericht designation	Prototype	[a]Model
Liquid	0 to 100					TSPIL
Bcc (U)	0 to 3	*cI2*	*Im-3m*	*Ab*	α-U	CEF
Tetragonal (U)	0 to 1	*tP30*	$P4_2/mmm$	*A2*	B-U	CEF
Orthorhombic (U)	0	*oC4*	*Cmcm*	*A20*	W	R-K/Muggianu
Diamond (Si)	100	*cF8*	*Fd-3m*	*A4*	C (Diamond)	R-K/Muggianu
U_3Si (High T)	75	*cP4*	*Pm-3m*	$L1_2$	Cu_3Au	ST
U_3Si (Low T)	75	*tI16*	*I4/mcm*	....	....	ST
U_3Si_2	~40 to ~41.5	*tP10*	*P4/mbm*	*D5a*	U_3Si_2	CEF
USi ($U_{68}Si_{67}$)	~50	....	*I4/mmm*	....	USi	ST
U_3Si_5	~61.5–~63	*hP3*	*P6/mmm*	*C32*	AlB_2	CEF
$USi_{1.84}$	64.5	*tI12*	$I4_1/amd$	C_c	$ThSi_2$	ST
USi_3	75	*cP4*	*Pm-3m*	$L1_2$	Cu_3Au	ST

[a]TSPIL, is the two sublattice partially ionic liquid model; ST, is stoichiometric compound and CEF, is the compound energy formalism. R-K/Muggiaun is the one sublattice Redlich-Kister Muggiaun solution model.

necessary to refer the Gibbs energy of all phases to the same reference point for each element. It is common practice to choose the reference state to be the most stable phase at 298.15 K, 10^5 Pa. The temperature of T_1 and T_2 determines the range of the power series. In this work, the molar Gibbs energy of the pure uranium and silicon are the recommended SGTE values compiled by Dinsdale (1991).

3.2.3 Stoichiometric phases

The molar Gibbs energies for stoichiometric phases can be described by using Eq. 4 where the standard Gibbs energy is equal to the standard enthalpy (see Eq. 5) minus the temperature times the standard entropy (see Eq. 6).

$$^{\circ}G_T = {}^{\circ}H_T - T{}^{\circ}S_T \tag{4}$$

$$^{\circ}H_T = \Delta^{298.15K}H_f^{\circ} + \int_{298.15\,K}^{T} C_p dT \tag{5}$$

$$^{\circ}S_T = \Delta^{298.15K}S_f^{\circ} + \int_{298.15\,K}^{T} \left(C_p/T\right) dT \tag{6}$$

3.2.4 Two sublattice partial ionic liquid (TSPIL) model

The partially ionic two sublattice model (Lukas et al., 2007) is used to model liquid phases as:

$(C_i^{+\nu_i})_P(A_j^{-\nu_j}, VaB_k^0)_Q$ where C, A, VA and B denotes cation, anion, vacancy, and neutrally charged specie, respectively. ν_i and ν_j represents the charge on the cation, C_i, and anion, A_j, species, respectively. Charge neutrality necessitates that Q and P varies according to Eqs 7, 8 respectively:

$$P = \sum_A \upsilon_A y_A + Q y_{VA} \tag{7}$$

$$Q = \sum_C \upsilon_C y_C \tag{8}$$

υ_A and y_A are the charge and site fractions of the anion species, A_j, and υ_C and y_C are the charge and site fraction of the cation species, C_i, respectively. In Eq. 9, the Gibbs energy of the ionic liquid is expressed as:

$$G_m = \sum\sum y_{C_i} y_{A_j} A{}^{\circ}G_{C_i:\,A_j} + Q\left(y_{Va}\sum y_{C_i}{}^{\circ}G_{C_i} + \sum y_{B_k}{}^{\circ}G_{B_k}\right) + RT\left[P\sum y_{C_i}\ln y_{C_i} + Q\left(\sum y_{A_j}\ln y_{A_j} + y_{Va}\ln y_{Va} + \sum y_{B_k}\ln y_{B_k}\right)\right] + {}^{E}G_m \tag{9}$$

Where $^{\circ}G_{C_i:\,A_j}$ is the Gibbs energy of formation for $\nu_i + \nu_j$ moles of atoms of the endmembers C_iA_j while $^{\circ}G_{C_i}$ and $^{\circ}G_{B_k}$ are the formation values for C_i and B_k.

3.2.5 Solid solutions

The compound energy formalism (CEF) was introduced by Hillert (2001) to describe the Gibbs energy of solid phases with sublattices. These phases have two or more sublattices and at least one of these sublattices has a variable composition. Ideal entropy of mixing is assumed on each sublattice. This model is generally used to model crystalline solids; but it can also be extended to model ionic liquids.

Here, a solution phases with two sublattices, (A,B)a (C,D)b, will be used as an example to illustrate the compound energy formalism. In this model, components A and B can mix randomly on the first sublattice, as do the components C and D on the second sublattice. a and b are the corresponding stoichiometric coefficients. Site fraction y_i^s (see Eq. 10) is introduced to describe the constitution of the phase and is defined as follows:

$$y_i^s = \frac{n_i^s}{N^s} \tag{10}$$

n_i^s is the number of component *i* on sublattice (s) and N^s is the total number of sites on the same sublattice. When vacancies are considered in the model, the site fraction becomes Eq. 11:

$$y_i^s = \frac{n_i^s}{n_{VA}^s + \sum_i n_i^s} \tag{11}$$

TABLE 4 Optimized thermodynamic parameters for the U-Si system.

Phase	Thermodynamic parameter (J/mol)	References
Liquid: (U^{+4}, Si^{+4}) (VA)	$G^{Liq}_{U+4:\ VA} = G^{Liq}_{U} - {}^{\circ}H^{SER}_{U} = G^{Liq}_{U}$	Dinsdale (1991)
	$G^{Liq}_{Si+4:\ VA} = G^{Liq}_{Si} - {}^{\circ}H^{SER}_{Si} = G^{Liq}_{Si}$	Dinsdale (1991)
	${}^{\circ}L_{U+4,Si+4:\ VA} = -185536.75 + 26.417124T$	Berche et al. (2009)
	${}^{1}L_{U+4,Si+4:\ VA} = -98477.584 + 52.787132T$	Berche et al. (2009)
	${}^{2}L_{U+4,Si+4:\ VA} = 47133.465 - 10.794531T$	This work
BCC_A2: (U, Si) (VA)	$G^{BCC_{A2}}_{U:\ VA} = G^{BCC_{A2}}_{U} - {}^{\circ}H^{SER}_{U} = G^{BCC_{A2}}_{U}$	Dinsdale (1991)
	$G^{BCC_{A2}}_{Si:\ VA} = G^{Diamond}_{Si} + 49999 + 22.5T$	This work
	${}^{\circ}L_{U,Si:\ VA} = -96136.807$	Berche et al. (2009)
Tetragonal_U: (U, Si)	$G^{Tetragonal}_{U} = G^{Tetragonal}_{U} - {}^{\circ}H^{SER}_{U} = G^{Tetragonal}_{U}$	Dinsdale (1991)
	$G^{Tetragonal}_{Si} = G^{Tetragonal}_{Si} - {}^{\circ}H^{SER}_{Si} = G^{Diamond}_{Si} + 4000$	Berche et al. (2009)
	${}^{\circ}L_{U,Si:\ VA} = -78915.524$	This work
Orthorhombic_A20: (U, Si)	$G^{Orthorhombic_{A20}}_{U} = {}^{\circ}H^{SER}_{U}$	Dinsdale (1991)
	$G^{Orthorhombic}_{Si} = G^{Orthorhombic}_{Si} - {}^{\circ}H^{SER}_{Si} = G^{Diamond}_{Si} + 4.2$	Wang et al. (2016)
	${}^{\circ}L_{U,Si:\ VA} = -78590 + 13.25T$	This Work
Diamond_A4: (U, Si)	$G^{Diamond_{A4}}_{U} = G^{Orthorhombic_{A20}}_{U} + 31860.9 + 0.2T$	This work
	$G^{Diamond_{A4}}_{Si} = {}^{\circ}H^{SER}_{Si}$	Dinsdale (1991)
	${}^{\circ}L_{U,Si:\ VA} = -100000 - 18^{*}T$	This work
D5A_U_3Si_2: $(U)_3(Si)_2$(Si, VA)	$G^{D5A_{U3Si2}}_{U:\ Si:\ VA} = G^{D5A_{U3Si2}}_{U:\ Si:\ VA} - 3{}^{\circ}H^{SER}_{U} - 2{}^{\circ}H^{SER}_{Si} = -189929 - 36T + 3G^{Orthorhombic_{A20}}_{U} + 2G^{Diamond_{A4}}_{Si}$	This work
	$G^{D5A_{U3Si2}}_{U:\ Si:\ Si} = G^{D5A_{U3Si2}}_{U:\ Si:\ Si} - 3{}^{\circ}H^{SER}_{U} - 3{}^{\circ}H^{SER}_{Si} = -202967 + 7T + 3G^{Orthorhombic_{A20}}_{U} + 3G^{Diamond_{A4}}_{Si}$	
	${}^{\circ}L_{U+4,Si+4:\ VA} = 1000 - 10.245T$	
	${}^{1}L_{U+4,Si+4:\ VA} = 32023 + 58.3232T$	
C32_U_3Si_5: $(U)_3(Si)_5$(Si, VA)	$G^{D5A_{U3Si5}}_{U:\ Si:\ VA} = G^{D5A_{U3Si5}}_{U:\ Si:\ VA} - 3{}^{\circ}H^{SER}_{U} - 5{}^{\circ}H^{SER}_{Si} = -354955.897 - 30T + 3G^{Orthorhombic_{A20}}_{U} + 5G^{Diamond_{A4}}_{Si}$	This work
	$G^{D5A_{U3Si5}}_{U:\ Si:\ Si} = G^{D5A_{U3Si5}}_{U:\ Si:\ Si} - 3{}^{\circ}H^{SER}_{U} - 3{}^{\circ}H^{SER}_{Si} = -222204.02 + 116.89T + 3G^{Orthorhombic_{A20}}_{U} + 3G^{Diamond_{A4}}_{Si}$	
	${}^{\circ}L_{U+4,Si+4:\ VA} = 5000 - 205.297T$	
	${}^{1}L_{U+4,Si+4:\ VA} = 90000 + 78.3232T$	
	${}^{1}L_{U+4,Si+4:\ VA} = 9800 + 10.215T$	
$U_{68}Si_{67}$	$G_{U68Si67} = G_{U68Si67} - 68{}^{\circ}H^{SER}_{U} - 67{}^{\circ}H^{SER}_{Si} = -56410000.288 - 672.027T + 68G^{Orthorhombic_{A20}}_{U} + 67G^{Diamond_{A4}}_{Si}$	This work
$U_{12}Si_{22}$	$G_{U12Si22} = G_{U12Si22} - 12{}^{\circ}H^{SER}_{U} - 22{}^{\circ}H^{SER}_{Si} = -1544000.01007 - 55T + 12G^{Orthorhombic_{A20}}_{U} + 22G^{Diamond_{A4}}_{Si}$	This work
U_3Si	$G_{U3Si} = G_{U3Si} - 3{}^{\circ}H^{SER}_{U} - {}^{\circ}H^{SER}_{Si} = -1544000.01007 - 55T + 3G^{Orthorhombic_{A20}}_{U} + G^{Diamond_{A4}}_{Si}$	This work
	$\Delta H^{\alpha\rightarrow\beta} = 12600 @ 1043K$	
USi_3	$G_{U3Si} = G_{USi3} - 3{}^{\circ}H^{SER}_{U} - {}^{\circ}H^{SER}_{Si} = -99650.289 - 16.79T + G^{Orthorhombic_{A20}}_{U} + 3G^{Diamond_{A4}}_{Si}$	This work

n^{s}_{VA} is the number of vacancies on sublattice (s). The site fraction can be transferred to mole fraction (x_i) using the Eq. 12 below:

$$x_i = \frac{\sum_s n^s y^s_i}{\sum_i n^s (1 - y^s_{VA})} \tag{12}$$

When each sublattice is only occupied by one component, then end-members of the phase are produced. In the present case, four end-members exist. They are AaCb, AaDb, BaCb and BaDb. The surface of reference ${}^{ref}G_m$ is expressed as in Eq. 13:

$${}^{ref}G_m = y^1 y^2 {}^{\circ}G_{A:\ C} + y^1 y^2 {}^{\circ}G_{A:\ D} + y^1 y^2 {}^{\circ}G_{B:\ C} + y^1 y^2 {}^{\circ}G_{B:\ D} \tag{13}$$

The ideal entropy (${}^{id}S_m$) and the excess free energy are expressed as follows in Eqs 14, 15, respectively:

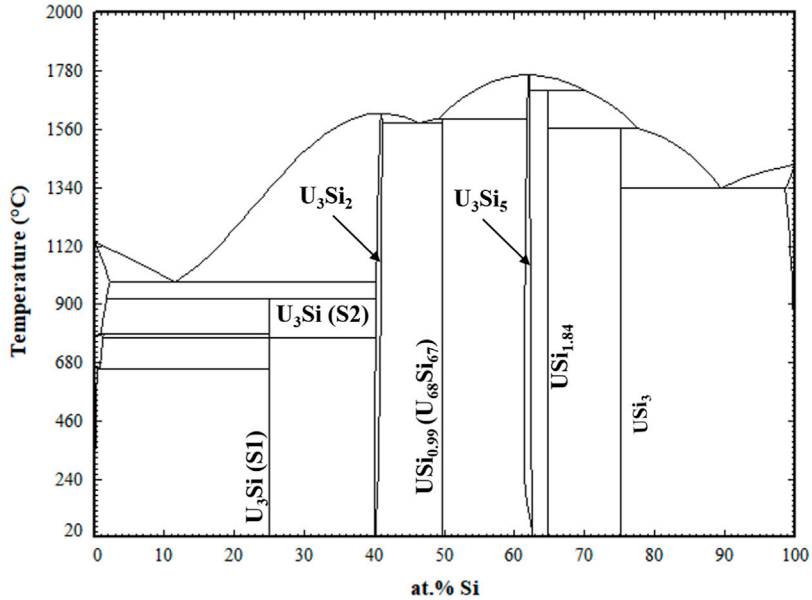

FIGURE 2
Optimized U-Si Phase Diagram. Arrows are pointing to the U_3Si_2 and U_3Si_5 homogeneity range.

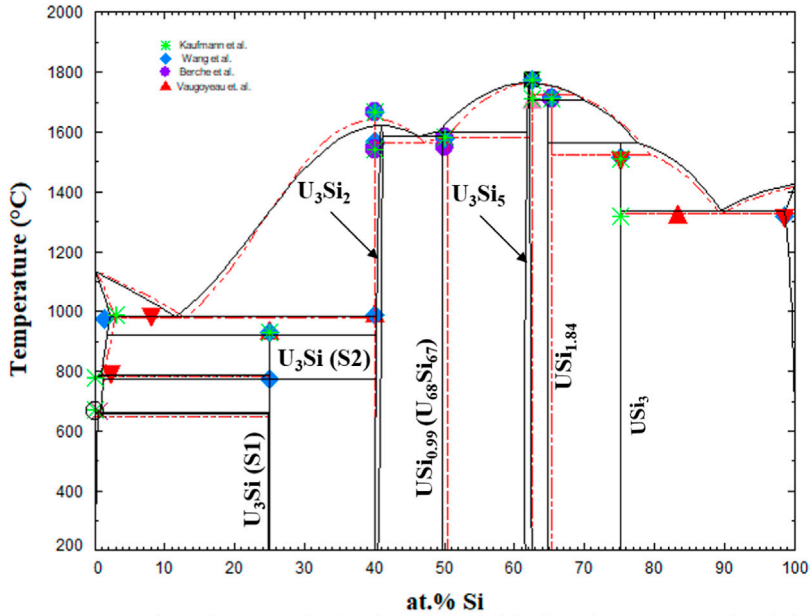

FIGURE 3
U-Si phase diagram calculated in the work (black) and super-imposed with the one from Berche et al., (Berche et al., 2009). The markers are experimental data from (Vaugoyeau et al., 1972; Dwight, 1982; Massalski, 1990; Wang et al., 2016).

$$^{id}S = -R[a(y_A^1 \ln y_A^1 + y_B^1 \ln y_B^1) + b(y_C^2 \ln y_C^2 + y_D^2 \ln y_D^2)] \quad (14)$$

$$^{E}G_m = y_A^1 y_B^1 (y_C^2 L_{A,B:\,D} + y_D^2 L_{A,B:\,D}) + y_C^2 y_D^2 (y_A^1 L_{A:\,C,D} + y_B^1 L_{B:\,C,D}) \quad (15)$$

The binary interaction parameters $L_{i,j:k}$ represent the interaction between the constituents i and j in the first sublattice when the second sublattice is only occupied by constituent k. These parameters can be further expanded with Redlich-Kister polynomial as follows in Eq. 16:

$$L_{i,j:\,k} = \sum_{\nu} \left(y_i^1 - y_j^1\right)^{\nu} L_{i,j:k} \quad (16)$$

In the case of a three sublattice model the Gibbs energy is written in Eq. 17 and the excess energy is given in Eq. 18:

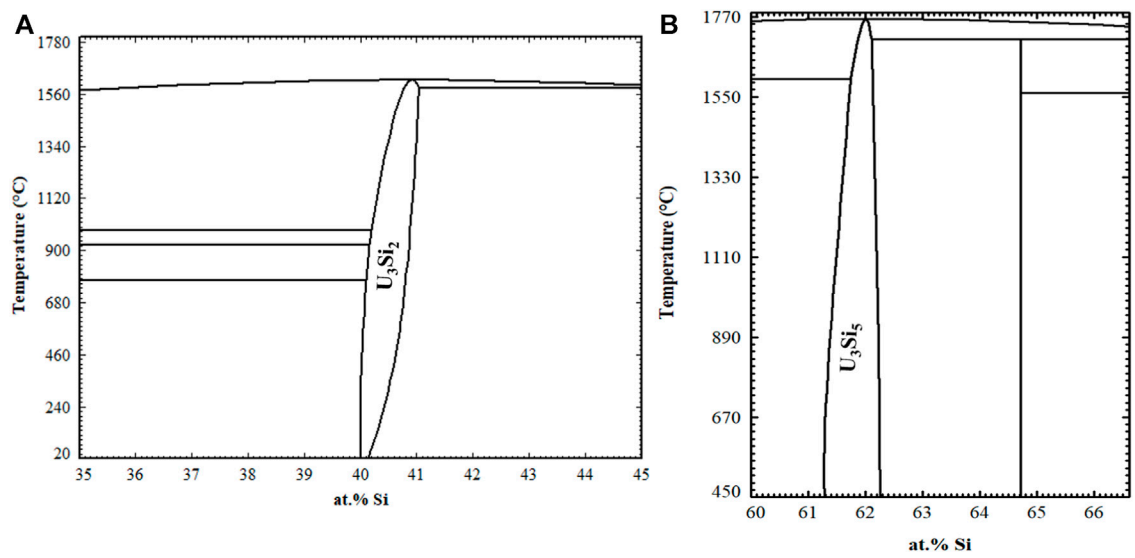

FIGURE 4
Zoomed in region of the U_3Si_2 **(A)** and U_3Si_5 **(B)** phase regions.

$$G_m = \sum_i y_i^I \sum_j y_j^{II} \sum_k y_k^{III} {}^{\circ}G_{i,j,k} + RT \sum_s \sum_i a^s y_i^s \ln y_i^s + {}^{E}G_m \tag{17}$$

$$\begin{aligned} {}^{E}G_m = {} & \sum_i y_i^I \sum_j y_j^{II} \sum_k y_k^{III} \Bigg[\sum_{l>i} y_l^I \sum_\nu {}^{\nu}L_{i,l:\,j:\,k} \left(y_i^I - y_l^I\right)^\nu \\ & + \Bigg[\sum_{l>j} y_l^{II} \sum_\nu {}^{\nu}L_{i,j:\,l:\,k} \left(y_j^{II} - y_l^{II}\right)^\nu \\ & + \Bigg[\sum_{l>k} y_l^{III} \sum_\nu {}^{\nu}L_{i,j:\,k:\,l} \left(y_k^{III} - y_l^{III}\right)^\nu \end{aligned} \tag{18}$$

4 Results

The FactSage thermochemical software (Bale et al., 2016) was used to perform the optimization of the uranium-silicon binary system. Summarized in Table 3 are the phases, with their crystal structure, space groups, prototypes, composition, and the thermodynamic model of the U-Si phases studied in this work. Unlike the previous two models (Berche et al., 2009; Wang et al., 2016), the liquid phase is modeled using the TSPIL model, where the first sublattice contains the U^{+4} and Si^{+4} cations and the second sublattice is occupied by a neutral vacancy as depicted by Eq. 19.

$$\left(U^{+4}, Si^{+4}\right)(VA) \tag{19}$$

This model was chosen because it is the mostly commonly used for modeling liquid phases and will therefore make incorporation of other elements into the U-Si database (e.g., fission product) a straightforward process. The excess energy parameters from Berche et al. (2009) were used for the initial point and adjusted as necessary.

The USi_3, $USi_{1.84}$, $U_{68}Si_{67}$, and U_3Si compositions were modeled as stoichiometric phases. The USi phase was previously assessed with the FeB-type structure; however, neutron diffraction confirmed that the phase has a tetragonal structure with *I4/mmm* space group. Therefore, the phase was modeled based on the recent findings. The recent enthalpy of formation data collected in 2018 (Chung et al., 2018) for the USi phase with tetragonal structure was used in the optimization. The composition of the USi_{2-x} phase was adjusted from $USi_{1.88}$ to $USi_{1.84}$ to reflect the experimental findings (Remschnig et al., 1992).

The U_3Si_5 and U_3Si_2 phases were modeled as a solid solution using the CEF model. The U_3Si_2 phase was modeled with 3 sublattices $(U)_3(Si)_2(Si, VA)$. Originally, a four sublattice model was applied to the system based on Wyckoff positions of the atoms; however, the model was simplified by adding a third sublattice to its stoichiometric representation (i.e., $(U)_3(Si)_2(Si, VA)$). This is justified as the nonstoichiometry in U_3Si_2 is primarily driven by silicon interstitials defects as shown by Ulrich et al. (2020b). Modeling the phase in this manner will facilitate modeling incorporation of light elements that are known to dissolve in the U_3Si_2 lattice such as hydrogen and carbon forms a U_3Si_2X phase (X = H or C). All one would need to do is add these elements to the third sublattice. The model can also be expanded on the first and second sublattices, which will be useful for CALPHAD assessment of fission products with U_3Si_2 fuel.

The U_3Si_5 phase was also modeled using CEF model with 3 sublattices, $(U)_3(Si)_5(Si, VA)$. Although, this phase could have been modeled using 2 sublattices by using the relationship; U_3Si_5 = AlB_2-type USi_{2-x}, modeling with the three sublattice was simpler as there is the $ThSi_2$-type USi_{2-x} structure (i.e., $USi_{1.84}$) close in composition to U_3Si_5, which makes the phase equilibria calculations more difficult.

The optimized parameters for the compounds and solid solutions are provided in Table 4 and the phase diagram is provided in Figure 2.

TABLE 5 Invariant reactions in the U-Si system calculated in the work and compared to literature values.

Reaction	Reaction type	Temperature (°C)	Composition (at. %U)			References
$liquid \leftrightarrow U_3Si_5$	Congruently melting	1770 ± 10			37.5	Kaufmann et al. (1957)
		~1700			37.5	Vaugoyeau et al. (1972)
		1773			37.5	White et al. (2015)
		1762			38	This work
$\alpha U_3Si \leftrightarrow \beta U_3Si$	Allotropic	770			75	Goddard et al. (2016)
		770			75	World Nuclear News (2019)
		769.85			75	This work
$liquid + U_3Si_5 \leftrightarrow USi$	Peritectic	1,580 ± 10		37.5	50	Dwight (1982b)
		1,576	~50	37.5	50	World Nuclear News (2019)
		1,597.4	51	38.3	50.4	This work
$liquid \leftrightarrow U_3Si_2$	Congruently melting	1,540 ± 10			60	Dwight (1982b)
		1,665			60	Dwight (1982b)
		1,664			60	World Nuclear News (2019)
		1,618.9			59.1	This work
$liquid + U_3Si_5 \leftrightarrow USi_{1.88}$	Peritectic	1710 ± 10		37.5	34.7	Dwight (1982b)
		1715	28.5	37.5	34.7	World Nuclear News (2019)
		1706.54	30.2	37.9	35.3	This work
$liquid \leftrightarrow bcc\,U + U_3Si_2$	Eutectic	985	92.1	98.4	60	White et al. (2017)
		985	88.5	98.2	60	World Nuclear News (2019)
		982.5	88.6	97.8	59.8	This work
$\beta U_3Si \leftrightarrow bcc\,U + U_3Si_2$	Eutectoid	930	75	98.2	60	White et al. (2017)
		929	75	98.6	60	World Nuclear News (2019)
$liquid \leftrightarrow dia.\,Si + USi_3$	Eutectic	1,315	10.7	1.4	25	Wang et al. (2016)
		1,317	9.7	1.1	25	World Nuclear News (2019)
		1,335.71	10.6	0.014	25	This work
$tetra\,U + \alpha U_3Si \leftrightarrow ortho\,U$	Eutectoid	665	~100	75	~100	White et al. (2017)
		665	~99.4	75	~99.5	World Nuclear News (2019)
$liquid + USi_{1.88} \leftrightarrow USi_3$	Peritectic	1,510 ± 10	19.1	34.7	25	Dwight, (1982b)
		1,511	17.8	34.7	25	World Nuclear News (2019)
		1,560.43	22.5	35.3	25	This work
$bcc\,U + \alpha U_3Si \leftrightarrow tetra\,U$	Eutectoid	795	98.6	75	97.7	White et al. (2017)
		794	99.4	75	98.7	World Nuclear News (2019)
		784.24	99.2	75	98.8	This work
$liquid \leftrightarrow U_3Si_2 + USi$	Eutectic	1,583.2	53.8	59.0	50.4	This work
$liquid \leftrightarrow dia.Si$	Melting	1,425.26			0	This work
$liquid \leftrightarrow bcc\,U$	Melting	1,134.84			100	This work
$bcc\,U + U_3Si_2 \leftrightarrow U_3Si$	Eutectoid	920.06	98.3	59.8	75	This work
$tetra\,U + U_3Si_2 \leftrightarrow U_3Si$	Eutectoid	769.85	98.8	59.9	75	This work
$tetra\,U \leftrightarrow ortho\,U + U_3Si$	Eutectoid	655.99	99.2	99.7	75	This work

5 Disscussion

The U-Si phase equilibria was modeled using the CALPHAD methodology and for the first time the U_3Si_2 and U_3Si_5 phases were modeled as nonstoichiometric phases using the 3 sublattice CEF model. The optimized diagram is displayed in Figure 3 and is compared to experimental data and calculated diagram by Berche *el. al.* (Berche et al., 2009). The diagram is in good agreement with respect to melting point and the terminal solutions.

Displayed in Figure 4 is a zoomed in region of the U_3Si_2 a) and U_3Si_5 b) phases. The U_3Si_2 phase is modeled with a homogeneity range of $U_3Si_{1.95}$ to $U_3Si_{2.05}$, which is in agreement with the neutron and experimental results from this project (Ulrich et al., 2020b); however, it disagrees with the work of Middleburg et al. (Middleburgh et al., 2016), at low temperatures (i.e., any temperature below 1,000°C). Further experimental work is suggested on samples with a wider homogeneity range to determine the exact width of the solubility range. However, this work shows that modeling the U_3Si_2 phase with the 3 sublattice model is sufficient enough to mimic the experimental composition. Furthermore, it will serve as a starting point for incorporating elements with the affinity for dissolving into U_3Si_2.

Experimentally, it has been shown that the U_3Si_5 phase can exist between the 62.5–63.4 at.% Si phase region; however, since it exists with an unknow, the exact composition of the phase is unknown. Although the phase diagram showed an overall good agreement with experimental data, the model for this phase could use further optimizing as the calculated composition region is narrower than the experimental composition. However, before further optimization of the phase, further experiments and computational analysis would prove useful for understanding the nature of the phase transition associated with the composition. The calculated enthalpy of formation for the stoichiometric compounds and the different invariant reactions are in agreement with literature values, see Table 2 and Table 5, respectively.

6 Conclusion

The aim of this work was to develop a self-consistent thermodynamic database for the uranium-silicon system that can be used to predict silicide fuel behavior during normal or off-normal reactor operations, optimize fuel fabrication processes, and support licensing efforts. To achieve this, the 40–66 at% Si region of the U-Si system had to be investigated for the phases, phase transitions, homogeneity ranges, and crystal structures.

A thermodynamic database for the U-Si phase containing the optimized parameters has been developed and an overall good agreement between the calculated diagram and the experimental phase diagram data was achieved. Representing the U_3Si_2 phase as a 3 sublattice model accurately accounts for Si interstitial defects, which are the primary defects found in this structure. The CALPHAD results for the phase diagram from 40–66 at% Si are summarized below.

- The U_3Si_2 phase exhibits a homogeneity range from room temperature to its melting point.
- U_5Si_4 (*P6/mmm* space group) should not be considered as an equilibrium phase in the U-Si system. The phase could potentially be metastable with negative energy of formation located 2 meV above the U-Si convex hull and has a stable isostructural ternary phase, $U_{20}Si_{16}C_3$ (*P6/mmm*). This suggests that the binary could be stabilized by a third element (Lopes et al., 2018; Kocevski et al., 2019; Ulrich et al., 2020a).
- The crystal structure of the USi phase was confirmed as having a tetragonal supercell with an *I4/mmm* space group and invariant stoichiometry of $USi_{0.99}$ (Ulrich et al., 2020a).
- Above 450°C, the U_3Si_5 phase was found to exhibit a homogeneity range. Below 450°C, U_3Si_5 was found to exist with another unidentified phase. Regarding the equilibrium phase diagram, it is recommended that this phase transition not be included until more knowledge is acquired.
- The composition of the tetragonal α-USi_2 phase was found to be ~$USi_{1.84}$ after annealing for 72 h at 1,200°C.
- The Molar mass of USi and $USi_{1.88}$ were adjusted to represent change in composition, $U_{68}Si_{67}$ and $USi_{1.84}$, respectively.

Data availability statement

The original contributions presented in the study are included in the article/Supplementary material, further inquiries can be directed to the corresponding author.

Author contributions

TU: Conceptualization, Data curation, Formal Analysis, Investigation, Methodology, Visualization, Writing–original draft, Writing–review and editing. TB: Conceptualization, Funding acquisition, Project administration, Resources, Writing–review and editing.

Funding

The author(s) declare financial support was received for the research, authorship, and/or publication of this article. The work done in this paper contributes to the project: Phase Equilibria and Thermochemistry of Advance Fuel: Modelling Burnup Behavior. This work was funded by the Department of Energy Nuclear Energy University Program (NEUP).

Acknowledgments

The authors would also like to acknowledge Sven C. Vogel, Joshua T. White, David A. Andersson, Elizabeth Sooby, Denise A. Lopes, Vancho Kocevski, and Emily Moore for their significant contribution to the project that helped to generate the data needed in order to perform a CALPHAD optimization.

Conflict of interest

The authors declare that the research was conducted in the absence of any commercial or financial relationships that could be construed as a potential conflict of interest.

Publisher's note

References

Alcock, C. B., and Grieveson, P. (1961). A thermodynamic study of the compounds of uranium with silicon, germanium, tin, and lead. *J. Inst. Metals* 90, 304–310.

Bale, C. W., Bélisle, E., Chartrand, P., Decterov, S. A., Eriksson, G., Gheribi, A. E., et al. (2016). FactSage thermochemical software and databases, 2010–2016. *CALPHAD* 54, 35–53. doi:10.1016/j.calphad.2016.05.002

Berche, A., Rado, C., Rapaud, O., Guéneau, C., and Rogez, J. (2009). Thermodynamic study of the U-Si system. *J. Nucl. Mater.* 389, 101–107. doi:10.1016/j.jnucmat.2009.01.014

Bihan, T. L., Noel, H., and Rogl, P. F. (1996). Crystal Structure of the uranium monosilicide (USi). *J. Alloys Compd.* 240, 128–133. doi:10.1016/0925-8388(96)02273-6

Birtcher, R. C., Mueller, M. H., Richardson, J. W., and Faber, J. (1989). Neutron irradiated uranium silicides studied by neutron diffraction and Rietveld analysis. *MRS Online Proc. Libr. Arch.* 166, 437. doi:10.1557/proc-166-437

Boucher, R. R. (1971). X-ray diffraction on U_3Si. *J. Acta Crystallogr.* 4, 326–328. doi:10.1107/S0021889871007088

Bragg-Sitton, S., Merrill, B., Teague, M., Ott, L., Robb, K., Farmer, M., et al. (2014). *Advanced fuels campaign: enhanced LWR accident tolerant fuel performance metrics*. United States: Idaho National Laboratory. Technical Report INL/EXT-13-29957.

Brauer, G., and Haag, H. (1949). Notiz über die Kristallstruktur von Uransilicid. *Z. Fur Anorg. Chem.* 259, 197–200. doi:10.1002/zaac.19492590117

Brown, A., and Norreys, J. (1961). Uranium disilicide. *Nature* 191, 61–62. doi:10.1038/191061a0

Brown, A., and Norreys, J. J. (1959). Beta-polymorphs of uranium and thorium disilicides. *Nature* 183, 673. doi:10.1038/183673a0

Carmack, J., Goldner, F., Bragg-Sitton, S. M., and Snead, L. L. (2013). *Overview of the U.S. DOE accident tolerant fuel development program, TopFuel 2013 Charlotte*. United States: Idaho National Lab. (INL), Idaho Falls.

Chung, C.-K., Guo, X., Wang, G., Wilson, T. L., White, J. T., Nelson, A. T., et al. (2018). Enthalpies of formation and phase stability relations of USi, U_3Si_5 and U_3Si_2. *J. Nucl. Mater.* 523, 101–110. doi:10.1016/j.jnucmat.2019.05.052

Cullity, B. D. (1945). Alloys of uranium and silicon. I. The uranium-silicon phase diagram. U.S.A.E., Report No. CT-3310.

Dinsdale, A. (1991). SGTE data for pure elements. *CALPHAD* 15, 317–425. doi:10.1016/0364-5916(91)90030-N

Dwight, A. (1982a). *Study of the uranium–aluminum–silicon system*. IL, USA: Argonne National Lab. doi:10.2172/6753243

Dwight, A. E. (1982b). *Study of the uranium-aluminum-silicon system*. United States: Argonne National Lab. doi:10.2172/6753243

Ferro, R., and Cacciamani, G. (2002). Remarks on crystallochemical aspects in thermodynamic modeling. *CALPHAD* 26, 439–458. doi:10.1016/S0364-5916(02)00056-1

Goddard, D. T., Mathers, D. P., Eaves, D. G., Xu, P., Lahoda, E. J., and Harp, J. M. (2016). *Manufacturability of U_3Si_2 and its high temperature oxidation behavior*. USA: Boise, Idaho.

Gross, T., Hayman, C., and Clayton, M. H. (1962). Thermodynamic of nuclear materials. *Process Symp.* 1963, 653–665.

Hillert, M. (2001). The compound energy formalism. *J. Alloys Compd.* 320, 161–176. doi:10.1016/S0925-8388(00)01481-X

Johnson, K. D., Raftery, A. M., Lopes, D. A., and Wallenius, J. (2016). Fabrication and microstructural analysis of UN-U_3Si_2 composites for accident tolerant fuel applications. *J. Nucl. Mater.* 477, 18–23. doi:10.1016/j.jnucmat.2016.05.004

Johnson, K. E., Adorno, D. L., Kocevski, V., Ulrich, T. L., White, J. T., Claisse, A., et al. (2020). Impact of fission product inclusion on phase development in U_3Si_2 fuel. *J. Nucl. Material* 537, 152235. doi:10.1016/j.jnucmat.2020.152235

Karoutas, Z., Brown, J., Atwood, A., Hallstadius, L., Lahoda, E., Ray, S., et al. (2018). The maturing of nuclear fuel: past to accident tolerant fuel. *Prog. Nucl. Energy* 102, 68–78. doi:10.1016/j.pnucene.2017.07.016

Katz, J. J., and Rabinowitch, E. (1951). *The chemistry of uranium – Part 1, the element, its binary and related compounds*. New York: McGraw-Hill Book Company, Inc., 226–229.

Kaufman, L., and Bernstein, H. (1970). *Computer calculations of phase diagrams*. New York: Academic Press.

Kaufmann, A. R., Cullity, B. D., and Bitsianes, G. (1957). Uranium silicon alloys. *J. Metals* 9, 23–27. doi:10.1007/BF03398440

Kim, H. G., Yang, J. H., Kim, W. J., and Koo, Y. H. (2016). Development status of accident tolerant fuel for light water reactors in Korea. *Nucl. Eng. Technol.* 48, 1–15. doi:10.1016/j.net.2015.11.011

Kim, Y. S. (2012). "Uranium intermetallic fuels (U-Al, U-Si, U-Mo)," in *Comprehensive nuclear materials*. Editor R. Konings, 3, 391–422.

Kimmel, G., Sharon, B., and Rosen, M. (1980). Structure and phase stability of uranium-silicon U_3Si at low temperatures. *Acta Crystallogr.* B36, 2386–2389. doi:10.1107/S0567740880008783

Kocevski, V., Lopes, D. A., and Besmann, T. M. (2019). Investigation of the on-site Coulomb correction and temperature dependence of the stability of U–Si phases using DFT+U. *J. Nucl. Mater.* 524, 157–163. doi:10.1016/j.jnucmat.2019.07.003

Kurata, M. (2016). Research and development methodology for practical use of accident tolerant fuel in light water reactors. *Nucl. Eng. Technol.* 48, 26–32. doi:10.1016/j.net.2015.12.004

Laugier, J., Blum, P. L., and de Tournemine, R. (1971). Sur la veritable structure du compose USi. *J. Nucl. Mater.* 41, 106–108. doi:10.1016/0022-3115(71)90205-4

Liu, Z. K. (2009). First principles calculations and calphad modeling of thermodynamics. *J. Phase Equilibria* 30, 517–534. doi:10.1007/s11669-009-9570-6

Lopes, D. A., Kocevski, V., Wilson, T. L., and Besmann, T. M. (2018). Stability of U_5Si_4 phase in U-Si system: crystal structure prediction and phonon properties using first-principles calculations. *J. Nucl. Mater.* 510, 331–336. doi:10.1016/j.jnucmat.2018.08.026

Lopes, D. A., Wilson, T. L., Kocevski, V., Moore, E. E., Besmann, T. M., Sooby Wood, E., et al. (2019). Experimental and computational assessment of USiN ternary phases. *J. Nucl. Mater.* 516, 194–201. doi:10.1016/j.jnucmat.2019.01.008

Lukachuk, M., and Pöttgen, R. (2003). Intermetallic compounds with ordered U_3Si_2 and Zr_3Al_2 type structure – crystal chemistry, chemical bonding and physical properties. *Z. für Kristallogr.* 218, 767–787. doi:10.1524/zkri.218.12.767.20545

Lukas, H., Fries, S. G., and Sundman, B. (2007). *Computational thermodynamics: the calphad method*. Cambridge: Cambridge University Press.

Massalski, B. T. (1990). *Binary alloy phase diagrams*. second Ed. (Materials Park, OH: ASM), 3374–3375.

Middleburgh, S. C., Grimes, R. W., Lahoda, E. J., Stanek, C. R., and Andersson, D. A. (2016). Non-stoichiometry in U_3Si_2. *J. Nucl. Mater.* 482, 300–305. doi:10.1016/j.jnucmat.2016.10.016

Noël, H., Chatain, S., Alpettaz, T., Guéneau, C., Duguay, C., and Léchelle, J. (2023). Experimental determination of (U-Si-C) ternary phase diagram at 1000°C and experimental points in the quaternary (U-Pu-Si-C) system. F-BRIDGE, Report No. D-151.

Noordhoek, M. J., Besmann, T. M., Andersson, D., Middleburgh, S. C., and Chernatynskiy, A. (2016). Phase Equilibria in the U-Si system from first-principles calculations. *J. Nucl. Mater.* 479, 216–223. doi:10.1016/j.jnucmat.2016.07.006

Noël, H., Queneau, V., Durand, J. P., and Colomb, P. (1998). *Abstract of a paper at the international conference on strongly correlated electron systems-SCSES98*, 92.

OHare, P. A. G., Hubbard, W. N., Johnson, G. K., and Settle, J. L. (1974). Thermodynamic of nuclear materials. *Process Symp. Vienna* 1975, 452.

Ott, H. R., Hulliger, F., Rudigier, H., and Fisk, Z. (1985). Superconductivity in uranium compounds with Cu_3Au structure. *Phys. Rev. B* 31, 1329–1333. doi:10.1103/physrevb.31.1329

Otto, R., and Kister, A. T. (1948). Algebraic representation of thermodynamic properties and the classification of solutions. *Industrial Eng. Chem.* 40 (2), 345–348. doi:10.1021/ie50458a036

Perrut, M. (2015). Thermodynamic modeling by the calphad method and its applications to innovative materials. *AerospaceLab* 9, 1–11.

Pöttgen, R. (1994). Ternary rare earth metal gold stannides and indides with ordered U3Si2 and Zr3Al2-type structure. *Verl. Z. für Naturforsch.* 49, 1525–1530. doi:10.1515/znb-1994-1112

Remschnig, K., LeBihan, T., Noël, H., and Rogl, P. (1992). Structural chemistry and magnetic behavior of binary uranium silicides. *J. Solid State Chem.* 97, 391–399. doi:10.1016/0022-4596(92)90048-Z

Sasa, Y., and Uda, M. (1976). Structure of stoichiometric USi_2. *J. Solid State Chem.* 18, 63–68. doi:10.1016/0022-4596(76)90079-7

Schindelin, J., Arganda-Carreras, I., Frise, E., Kaynig, V., Longair, M., Pietzsch, T., et al. (2012). Fiji: an open-source platform for biological-image analysis. *Nat. Methods* 9, 676–682. doi:10.1038/nmeth.2019

Terrani, K. (2018). Accident tolerant fuel cladding development: promise, status, and challenges. *J. Nucl. Mater.* 501, 13–30. doi:10.1016/j.jnucmat.2017.12.043

Toby, B. H., and Von Dreele, R. B. (2013). GSAS-II: the genesis of a modern open-source all-purpose crystallography software package. *J. Appl. Crystallogr.* 46, 544–549. doi:10.1107/S0021889813003531

Ulrich, T. L. (2019). "Modeling the uranium-silicon phase equilibria based on computational and experimental analysis," (South Carolina: University of South Carolina). (Doctoral dissertation).

Ulrich, T. L., Vogel, S. C., Lopes, D. A., Kocevski, V., White, J. T., Sooby, E. S., et al. (2020a). Phase stability of U_5Si4, USi, and U_2Si_3 in the uranium–silicon system. *J. Nucl. Mater.* 540, 152353. doi:10.1016/j.jnucmat.2020.152353

Ulrich, T. L., Vogel, S. C., White, J. T., Andersson, D. A., Sooby Wood, E., and Besmann, T. M. (2020b). High temperature neutron diffraction investigation of U_3Si_2. *Materialia* 9, 100580. doi:10.1016/j.mtla.2019.100580

U.S Department of Energy (2015). Development of Light Water Reactor fuels with enhanced accident tolerance. Report to Congress.

US Nuclear Regulatory Commission (2011). Special report on the accident at the Fukushima Diiachi nuclear power station. Report No. INP0 11-005.

Vaugoyeau, H., Lombard, L., and Morlevat, J. (1972). A contribution to the study of the uranium–silicon equilibrium diagram. Report No. AECL-4151.

Vooght, D.De., Verniers, G., and Meester, P.De. (1973). Counter-diffractometer parameter determination of polycrystalline U_3Si. *J. Nucl. Mater.* 46, 303–308. doi:10.1016/0022-3115(73)90045-7

Wang, J., Wang, K., Chunhua, M., and Xie, L. (2016). Critical Evaluation and thermodynamic optimization of the (U+Bi), (U+Si) and (U+Sn) binary systems. *J. Chem. Thermodyn.* 92, 158–167. doi:10.1016/j.jct.2015.08.029

Westinghouse (2023). Westinghouse's Encore fuel inserted in Exelon generation's Byron unit 2. Available at: http://www.westinghousenuclear.com/uknuclear/about/news/view/westinghouse-s-encore-fuel-inserted-in-exelon-generation-s-byron-unit-2.

White, J. T., Nelson, A. T., Byler, D. D., Valdez, J. A., and McClellan, K. J. (2014). Thermophysical properties of U_3Si to 1150 K. *J. Nucl. Mater.* 452, 304–310. doi:10.1016/j.jnucmat.2014.05.037

White, J. T., Nelson, A. T., Dunwoody, J. T., Byler, D. D., and McClellan, K. J. (2016). Thermophysical properties of USi to 1673 K. *J. Nucl. Mater.* 471, 129–135. doi:10.1016/j.jnucmat.2016.01.013

White, J. T., Nelson, A. T., Dunwoody, J. T., Byler, D. D., Safarik, D. J., and McClellan, K. J. (2015). Thermophysical properties of U_3Si_2 to 1773 K. *J. Nucl. Mater.* 464, 275–280. doi:10.1016/j.jnucmat.2015.04.031

White, J. T., Travis, A. W., Dunwoody, J. T., and Nelson, A. T. (2017). Fabrication and thermophysical property characterization of UN/U_3Si_2 composite fuel forms. *J. Nucl. Mater.* 495, 463–474. doi:10.1016/j.jnucmat.2017.08.041

Wilson, T. L., Moore, E. E., Lopes, D. A., KocevskiSooby Wood, V. E., White, J. T., Nelson, A. T., et al. (2018). Uranium nitride-silicide advanced nuclear fuel: higher efficiency and greater safety. *Adv. Appl. Ceram.* 117, S76–S81. doi:10.1080/17436753.2018.1521607

World Nuclear News (2019). US begins first commercial testing of silicide fuel. Available at: http://world-nuclear-news.org/Articles/US-begins-first-commercial-testing-of-silicide-fuel.

Zachariasen, W. H. (1949). Crystal chemical studies of the 5*f*-series of elements. VIII. Crystal structure studies of uranium silicides and of $CeSi_2$, $NpSi_2$, and $PuSi_2$. *Acta Crystallogr.* 2, 94–99. doi:10.1107/s0365110x49000217

Zinkle, S. J., and Was, G. S. (2013). Materials challenges in nuclear energy. *Acta Mater.* 61, 735–758. doi:10.1016/j.actamat.2012.11.004